



# Effect of Tip Roundness on the Nanoindentation of Fe Crystals

M. Clara Zonana<sup>1</sup> · Carlos J. Ruestes<sup>2</sup> · Eduardo M. Bringa<sup>3,4</sup> · Herbert M. Urbassek<sup>5</sup>

Received: 26 December 2019 / Accepted: 18 March 2020 / Published online: 7 April 2020  
© Springer Science+Business Media, LLC, part of Springer Nature 2020

## Abstract

Indentation tips are never atomically sharp, but rounded at their end. We use atomistic simulation to study the effect of tip roundness for the particular case of a cube-corner pyramidal indenter by comparing the results of a spherical, a sharp cube-corner, and a rounded cube-corner tip during indentation into bcc Fe. We find that as soon as the tip has indented so deeply that the spherical geometry does not hold any longer, strong deviations between the dislocation plasticity behavior show up. The rounded cube-corner tip produces less dislocations and a smaller plastic zone than the spherical indenter, when indented to the same depth. The results are better comparable, however, when the same displaced volume is considered. Finally, the dislocation nucleation mode is affected by the geometry, changing from homogeneous to heterogeneous nucleation as the tip changes from rounded to sharp. The cube-corner tips are found to produce more twinning and delay the formation of prismatic loops. For a penetration depth beyond the radius of the rounded cube-corner tip, atomic sharp pyramidal tips produce similar quantitative (hardness, dislocation density) and qualitative (pileup, dislocation arrangement) results compared to its rounded counterpart. Our results will prove important for understanding the differences between spherical indenter tips, as they are often used in simulation, and pyramidal tips, as they are used in experiment.

**Keywords** Molecular dynamics · Nanoindentation · Dislocations · Plasticity

**Electronic supplementary material** The online version of this article (<https://doi.org/10.1007/s11249-020-01295-9>) contains supplementary material, which is available to authorized users.

✉ Carlos J. Ruestes  
cruestes@fcen.uncu.edu.ar

Herbert M. Urbassek  
urbassek@rhrk.uni-kl.de  
<http://www.physik.uni-kl.de/urbassek/>

<sup>1</sup> Facultad de Ciencias Exactas y Naturales, Universidad Nacional de Cuyo, Padre J. Contreras 1300, 5500 Mendoza, Argentina

<sup>2</sup> Instituto Interdisciplinario de Ciencias Básicas, Universidad Nacional de Cuyo, CONICET and Facultad de Ciencias Exactas y Naturales, Padre J. Contreras 1300, 5500 Mendoza, Argentina

<sup>3</sup> CONICET, Facultad de Ingeniería, Universidad de Mendoza, 5500 Mendoza, Argentina

<sup>4</sup> Centro de Nanotecnología Aplicada, Facultad de Ciencias, Universidad Mayor, Providencia, Chile

<sup>5</sup> Physics Department and Research Center OPTIMAS, University Kaiserslautern, Erwin-Schrödinger-Straße, 67663 Kaiserslautern, Germany

## 1 Introduction

Nanoindentation has proven to be a technique of great versatility in materials science [1–4]. Its range of application includes the determination of the elastic modulus and hardness of a material, as well as fracture toughness, adhesion, strain hardening, etc. Atomistic studies based on molecular dynamics (MD) simulations offer the possibility to determine the hardness theoretically and have provided valuable insights into the deformation mechanisms taking place during nanoindentation; these include the generation, movement, and reactions of dislocations as well as twinning [5–8]. This method has been used extensively for studying a variety of materials, in particular, for metals. Here, most frequently, fcc metals [9–21] have been studied, and bcc [6, 21–31] and hcp [32, 33] crystals have been studied less frequently. Some examples are also found for metallic glasses [34] and high-entropy alloys [35]. Such simulations report on hardness values, extension of the plastic zone, pileup, and the defects generated.

The vast majority of nanoindentation molecular dynamics studies have explored the mechanical response of materials by focusing on the deformation mechanisms of the

substrate. In such studies, the indenter is often modeled as a smooth, rigid, and massless body. This is done by using a purely repulsive potential to mimic the tip and lacks of any atomistic description [36]. Such method is of extended use in the community of nanoindentation atomistic simulations and its concept originates from continuum mechanics, as it is akin to a Hertzian indenter. In a lesser amount and after the seminal work by Landman et al. [37], some relevant studies had employed atomistically resolved spherical indenters. Luan and Robbins [38] explored the breakdown of continuum models for contacts at the nanoscale by means of MD simulations, pointing out that it is not so much the atomic discreteness, but the atomic-scale surface roughness that may lead to deviations from continuum theory. Wagner et al. [39] reported a change from homogeneous to heterogeneous dislocation nucleation after changing from a smooth to an atomistically rough indenter. Another prominent example is the work by Hagelaar et al. [22] who used a deformable tungsten tip to probe a tungsten substrate.

In experiments, various forms of indenter tips are used, among which are a variety of cones and pyramids. Some attempts can be found in the MD literature to mimic such geometries; these include blunt cones [22], sharp cones [40], sharp pyramids [8, 41], including Berkovich-type sharp tips [8], blunt pyramids [42], cube-corner tips [26], and even a conosphere [43]. Simulations with such a variety of tips are often used to address some fundamental issues like the influence of tip geometry on hardness measurements, deformation mechanisms, and pileup formation.

A strong justification for the generalized use of a spherical tip shape in simulation is that on the nanoscale, all indenters (cones, pyramids, etc) are rounded at their tip and, as a consequence, one could expect that a sphere of similar radius to that of the experimental tip would provide a reasonable approximation to the real tip. Our objective in this study is to question such hypothesis and explore the influence of indenter shape and radius of the tip on the mechanics of nanocontact. For that purpose, in this paper, we study the nanoindentation of an Fe surface using atomistic indenters with three different tip geometries: a sphere, a cube-corner, and a rounded cube-corner tip. We choose to study a cube-corner tip due to a variety of reasons: (a) it is less studied than the Berkovich tip; (b) it is recommended for probing ultra-thin substrates; and (c) it has a smaller semi-angle at the faces ( $35.26^\circ$ ) compared to the Berkovich tip ( $70.3^\circ$ ), allowing for smaller substrates to be simulated.

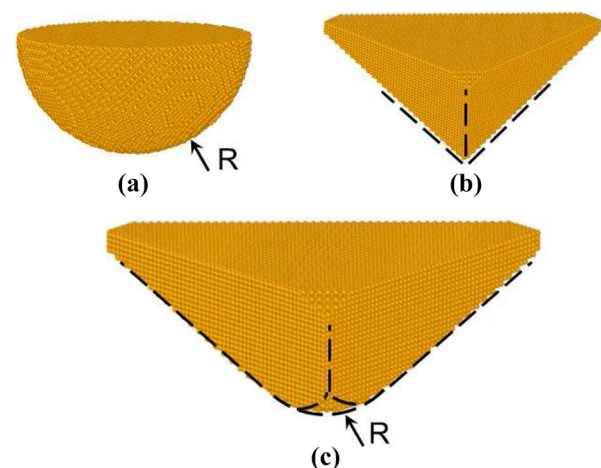
The description of the tips together with the simulation methods are described in Sect. 2. The results are presented in Sect. 3, including loading curves (Sect. 3.1), pileup formation, deformation mechanisms, and extension of the plastic zone (Sect. 3.2). The implications of our results are discussed on Sect. 4 and the main conclusions are outlined in Sect. 5.

## 2 Method

We employ molecular dynamics nanoindentation simulations to study the behavior of an iron single crystal using tips with different geometry.

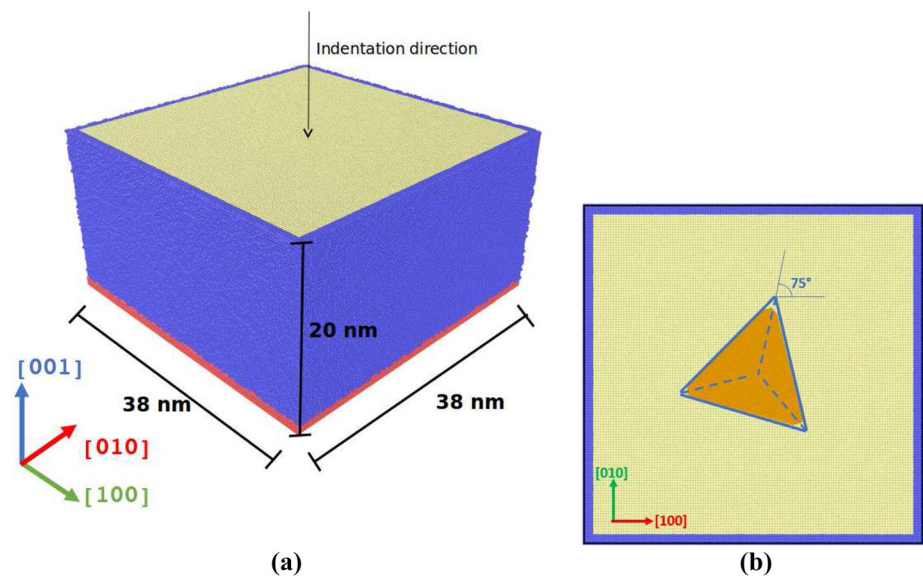
Figure 1 shows a schematic representation of the different tips tested; a sphere with a radius of  $R = 5$  nm, a sharp cube-corner with sides 9.5 nm, and a rounded cube-corner pyramid with the same radius as the spherical indenter. The cube corner was rounded such that the  $R = 5$  nm sphere was tangent to the cube edges. The sphere thus ends at a height of around  $7 \text{ \AA}$  above the tip bottom; above that height, the cube-corner geometry takes over. These are atomistic tips and all three indenters are composed of C atoms arranged in a rigid diamond lattice structure. The indentation axis is centered with respect to the substrate and in all cases; the initial position of the indenter is  $6.3 \text{ \AA}$  above the substrate. Such separation guarantees no tip–substrate interactions prior to indentation.

Figure 2a shows a schematic representation of the substrate together with (b) the orientation of the pyramidal tip with respect to the substrate. Periodic boundary conditions were applied in the  $x$  and  $y$  directions. The Fe substrate has dimensions of  $38 \times 38 \times 20 \text{ nm}^3$ , for a total of  $\approx 2$  million atoms. (100)-oriented bcc iron single crystal substrates were tested. The proximity of the simulation boundaries may affect MD simulation results [44]. In order to prevent such effects, we checked that the box is large enough to avoid the generated plasticity (dislocations) to reach the boundaries of the simulation box. The Fe–Fe interaction is described by the Mendeleev potential [45]. The interaction between the C atoms of the diamond indenter and the Fe



**Fig. 1** Shapes used for the atomistic indenters. **a** Sphere ( $R = 5$  nm). **b** Sharp cube-corner. **c** Rounded cube-corner ( $R = 5$  nm)

**Fig. 2** **a** Setup of the simulation system. The substrate has thermostating and rigid zones at its boundaries. **b** Orientation of the pyramidal tip with respect to the substrate



atoms of the substrate is modeled by means of a Lennard-Jones potential [46].

Before performing the indentation simulations, the substrates are initially minimized via conjugate gradient method [47]. After minimization, the samples are first equilibrated at zero pressure and at a temperature of 293 K for 20 ps through a NPT ensemble such that the cell dimensions are allowed to vary independently. In the x and y directions, the pressure is controlled by a barostat, while in the z direction, the pressure is held at zero by the absence of periodicity. Following the initial NPT run, a second equilibration of 20 ps using a NVE ensemble is carried out using boundary conditions that will also be used during the indentation process, as shown in Fig. 2.a. In this second equilibration, the barostat is turned off. In order to suppress any rigid-body movement of the substrate, two atom layers at the bottom of the substrate are fixed. The next four layers at the bottom and the sides are kept at a constant temperature of 293 K by means of a Langevin thermostat. At the end of the minimization and equilibration cycle, all stress components have reached values  $< 10^{-5}$  GPa [19].

The indenter tip penetration rate is chosen as 10 m/s. This velocity, though high compared to experimental indentation, is well below the longitudinal wave velocity of iron and should be considered low enough for typical MD studies. Gao et al. [21] studied the influence of indentation speed on a Fe (100) surface, showing that speeds in the range of the one used here provide low variation of results in terms of the extension of the plastic zone, whereas indentation speeds of the order of 100 m/s affect the development of plasticity by suppressing dislocation activity. Ruestes et al. [6] and Alcalá et al. [24] performed MD simulations of bcc Ta nanoindentation for velocities of 3.4–34 m/s and 4–0.004

m/s, respectively; they report that the plasticity mechanisms showed no significant differences in this velocity range.

The MD simulations are performed using the open-source LAMMPS code [48] with a constant time step of 1 fs. Visualization is performed using OVITO [49]; DXA [50] and CAT [51–53] are employed for analysis of the plasticity generated.

## 3 Results

### 3.1 Forces

Figure 3a displays the evolution of the normal forces for the three indenters tested. Here and in the following figures, the value of indentation depth = 0 applies when the first atom of the indenter tip is at the height of the top layer of the crystal. The loading curve for the spherical indenter is similar to previous MD studies of spherical indentation, with an elastic regime ending in an abrupt load drop for an indentation depth of 10 Å. This indication of a pop-in is consistent with a sudden stress relief due to nucleation of plasticity below the indenter, confirming previous experimental [54] and simulation findings [6, 24, 55].

For the sharp cube-corner indenter, the loading curve is quite different. This obeys, primarily, the acute shape of the tip, which produces an earlier departure from the elastic regime, due to the heterogeneous nucleation of plasticity at the surface. As the stress build-up is less prominent in this case, the load is systematically lower compared to that of the other two indenters. Lying in between the two aforementioned cases, the rounded cube-corner indenter offers a loading curve that appear to match that of the spherical indenter up to an indentation depth of 5 Å, where

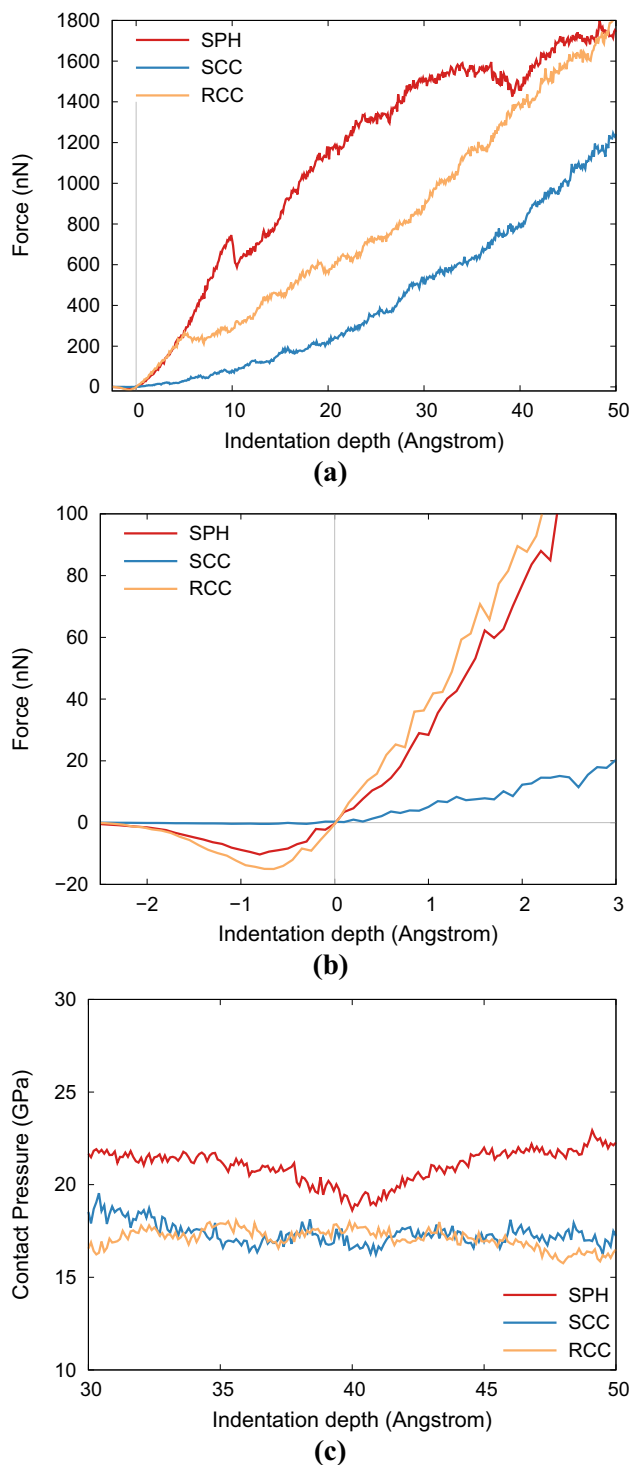


**Fig. 3** Loading curves for the three indenters tested. **a** Complete loading curves. **b** Zoom for an indentation depth up to 3 Å. **c** Evolution of contact pressures. *SPH* spherical indenter, *SCC* sharp cube-corner indenter, *RCC* rounded cube-corner indenter

the loading suffers a sudden change in slope, albeit without the marked load drop of the spherical indenter. In this case, the nucleation of plasticity is again homogeneous. The initial part of the curve is ruled by the spherical nature

of the tip; in fact, it follows the loading curve of the spherical tip. The plastic stage evolves with a slope markedly similar to that of the sharp cube-corner tip, signaling the dominance of the pyramidal shape in this stage.

The atomistic nature of the indenters used allows for exploration of the early stages of contact, as seen on Fig. 3b. It is clear that as the spherical and rounded cube-corner indenter approach the surface, the recorded loading curve goes to negative values. This is due to substrate exerting an attractive force on the tips, its effect being maximum for an indenter position slightly above the surface ( $-0.8$  Å) and the phenomena is a consequence of the attractive part of the interatomic potential. Such signatures are also present in experimental studies, such as in the atomic force microscopy measurements by Landman et al. [37]. The effect is unnoticeable for the sharp cube-corner tip, due to the extremely small amount of atoms that interact with the substrate atoms within their cutoff distance, before contact.

Figure 3c presents the evolution of contact pressure the last 30 Å of penetration. For such depths, the (instantaneous) contact pressure, which is defined as the ratio of the force and the respective projected contact area, stays rather constant after the onset of plasticity has been passed. The hardness of the material is defined as the contact pressure which has been established after the initial stages of plasticity, such that it stays rather constant with increasing indentation. Fluctuations in this regime are due to the atomistic resolution of the processes and immediately reflect the generation and interaction of dislocations with each other. Averaging over the fluctuations on Fig. 3c renders a hardness of 21.1 GPa for the spherical indenter, 17.4 GPa for the sharp cube-corner indenter, and 16.7 for the rounded cube-corner indenter. The results show that for the spherical indenter, the contact pressure is systematically higher than that for the cube-corner indenters, with values in the range of 18.6–23.2 GPa for the former and values in the range of 15.1–19.6 GPa for the latter. These results are in agreement with the literature; Gao et al. [30] obtained an average hardness of 19.7 GPa in their MD simulations of Fe (100) surface under spherical nanoindentation, while Alhafez et al. [40] obtained an average indentation hardness of around 16 GPa for a 30° semi-apex angle conical indenter and around 18.5 GPa for a 45° semi-apex angle conical indenter probing an iron (100) surface. Sustained high pressures on iron can lead to solid–solid phase transitions. Due to the high strain rates used in nanoindentation MD simulations, the transformation kinetics require pressures much higher than the thermodynamic standard value for the  $\alpha - \epsilon$  phase transition. Future studies might consider interatomic potentials that reproduce this transition at high pressures [56].



### 3.2 Pileup, Deformation Mechanisms, and Plastic Zone

Figure 4 presents the pileups generated by the spherical tip and the two cube-corner tips, for the same displaced volume. As expected, the pileups are distinctively different. The spherical indenter produced a pileup with a fourfold symmetry and a slight anisotropy, in agreement with previous MD studies on bcc metals [21] and experimental studies with spherical indenters on Ta and W [23, 57]. A fourfold symmetry is expected after spherical indentation of a (100) surface in a cubic crystal because of the fourfold symmetry of  $\langle 111 \rangle$  slip in this case. The cube-corner tips produced a markedly different pileup due to the different symmetry of the indenter with respect to the available slip systems. On the top, left hand side part of the pileup, material protruded in a larger extent compared to the other two planes of the tip. This is due to the angle formed by the plane (Figs. 2b, 4), whose normal vector is close to the  $[\bar{1}\bar{1}\bar{1}]$  direction, which facilitates the activation of slip systems on  $\{110\}$ ,  $\{112\}$ , and  $\{123\}$  slip planes with the same  $[\bar{1}\bar{1}\bar{1}]$  slip direction. The other two planes forming the cube-corner tips have normal vectors with a noticeable misorientation with respect to bcc slip vectors, which makes dislocation slip less favorable compared to the previous case and, as a consequence, the pileup is less pronounced in that region. The pileups formed by the pyramidal indenters are similar to the experimental pileups reported by Smith et al. [26] in their cube-corner nanoindentation studies of defect generation and pileup formation for Fe single crystals.

Figure 5 presents the defective structures below the surface corresponding to the pileups depicted in Fig. 4. Analysis of the defective structures reveals the generation of dislocations with two different kinds of Burgers vectors,  $\mathbf{b} = 1/2\langle 111 \rangle$  and  $\mathbf{b} = \langle 100 \rangle$ ; these dislocations

are plotted distinctly in Fig. 5, with green for the former and magenta for the latter. These dislocations are a typical response of bcc substrates [7]. Although dislocations with  $\mathbf{b} = 1/2\langle 111 \rangle$  Burgers vector have lower energy,  $\mathbf{b} = \langle 100 \rangle$  dislocations may form during deformation by the reaction between dislocations with Burgers vector  $\mathbf{b} = 1/2\langle 111 \rangle$  [30, 58, 59]. This can be noticed on several regions of Fig. 5 where two  $\mathbf{b} = 1/2\langle 111 \rangle$  (green) dislocations are reacting to form  $\mathbf{b} = \langle 100 \rangle$  (magenta) dislocations. For the spherical indenter, we note the generation of prismatic dislocation loops by the “lasso” mechanism [5]. Study of the defective structures for the rounded cube-corner tip also shows prismatic loops, but at a larger depth (50 Å) compared to the spherical case. Quantification of dislocation junctions by means of the Crystal Analysis Tool reveals that while the spherical and rounded cube-corner tip produce a similar amount of junctions, the sharp cube-corner tip generates 35 % more junctions at maximum penetration.

The evolution of the total length of dislocations  $L_{\text{disl}}$  as well as the total length of  $\mathbf{b} = 1/2\langle 111 \rangle$  dislocations was calculated by DXA and the results are presented on Fig. 6. The plots provide a quantitative representation of the phenomena explained in the preceding paragraphs. After nucleation, dislocation length increases with penetration. As it can be seen after the atomistic views (Fig. 5) and dislocation length calculations,  $\mathbf{b} = 1/2\langle 111 \rangle$  dislocations account for the vast majority of dislocations present.

The dislocation density,  $\rho$ , can be computed by the ratio of  $L_{\text{disl}}$  to the volume of the plastic zone  $V_{\text{pl}}$ ,

$$\rho = \frac{L_{\text{disl}}}{V_{\text{pl}}} \quad (1)$$

The volume of the plastic zone is considered to be of hemispherical form and is obtained by

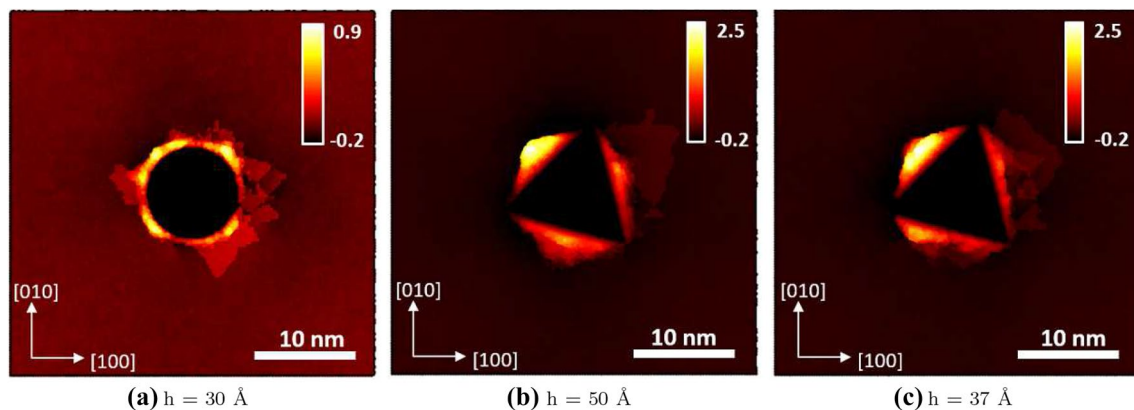


**Fig. 4** Pileup formed by spherical and cube-corner tips for the same displaced volumes (different indentation depth). Positive values denote height above the original surface plane. Note the different height scale in each case. The height scale is chosen to enhance visualization

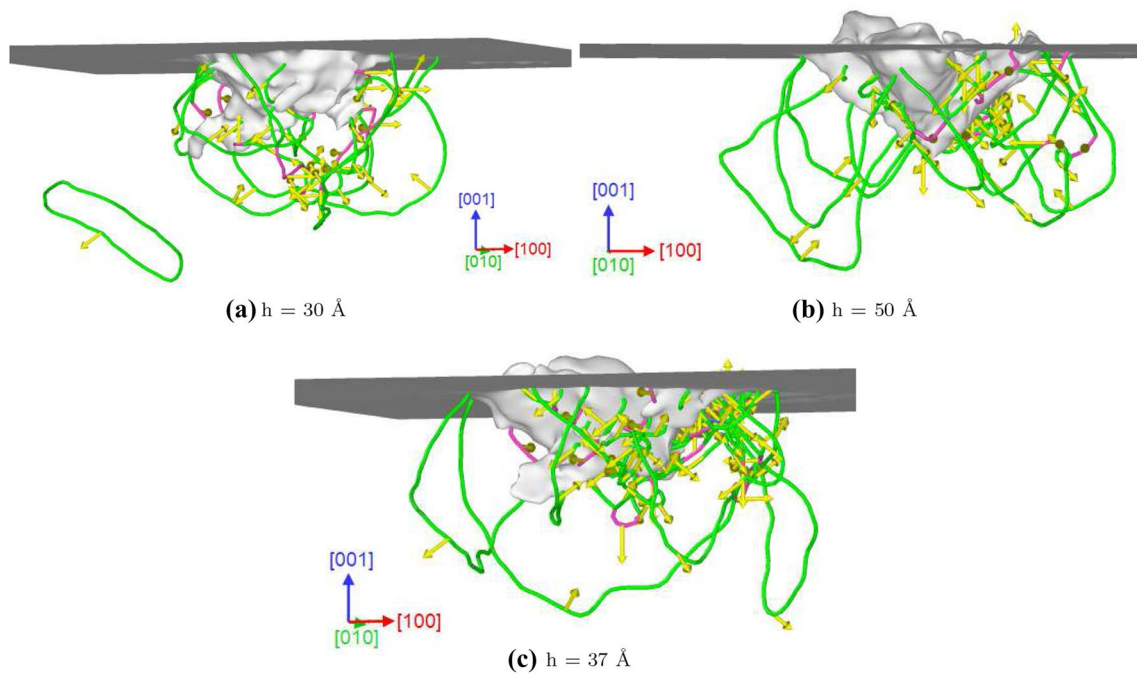


**Fig. 5** Defective structures below the surface for a condition of equal displaced volume (different indentation depth  $h$ ). **a** Spherical indenter. **b** Sharp cube-corner indenter. **c** Rounded cube-corner indenter

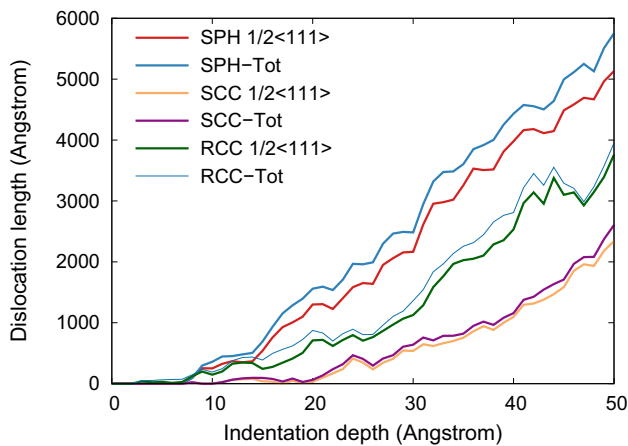


**Fig. 6** Evolution of total dislocation density and  $1/2\langle 111 \rangle$  dislocations for the three indenters tested

$$V_{pl} = \frac{2\pi}{3} R_{pl}^3 - V_{indent} \tag{2}$$

where the volume of the immersed part of the indenter,  $V_{indent}$ , is subtracted from the hemispherical plastic zone volume. The extension of the plastic zone ( $R_{pl}$ ) is computed following the methods and criteria presented elsewhere [21] and the results are reported in Tables 1 and 2.

In order to obtain estimates of the dislocation densities, two different criteria were chosen. As a first case, Table 1

**Table 1** Dislocation characteristics corresponding to the curves presented in Fig. 6 at an indentation depth of 40 Å

Indenter	$L_{disl}$ (nm)	$R_{pl}$ (nm)	$\rho$ ( $10^{16} \text{ m}^{-2}$ )
SPH	375.7	18.5	2.8
SCC	115.9	11.6	3.7
RCC	280.6	16.7	2.9

$L_{disl}$ : Total dislocation length.  $R_{pl}$ : Radius of plastic zone.  $\rho$ : Dislocation density

**Table 2** Dislocation characteristics corresponding to the curves presented in Fig. 6 for the same displaced volume

Indenter	$L_{disl}$ (nm)	$R_{pl}$ (nm)	$\rho$ ( $10^{16} \text{ m}^{-2}$ )
SPH ( $h = 30 \text{ \AA}$ )	227.5	15.9	2.7
SCC ( $h = 50 \text{ \AA}$ )	261.8	15.8	3.2
RCC ( $h = 37 \text{ \AA}$ )	269.0	15.4	3.5

$h$  denotes indentation depth. Notation as in Table 1

presents the results for each indenter is at the same indentation depth (40 Å). The results show that for the same indentation depth, the radius of the plastic zone is, roughly, 10 % smaller for the rounded cube-corner tip compared to that of the spherical indenter, while for the sharp cube-corner tip, the plastic zone is around 40 % smaller than that corresponding to the spherical tip. It is due to this considerable

difference that, despite introducing the smallest dislocation length, the sharp tip produces the highest dislocation density. As a second case, Table 2 presents the results for each indenter considering an equal displaced volume, corresponding to Figs. 4 and 5. The results show that for the same displaced volume, the radius of the plastic zone is quite similar among the three cases, where the cube-corner tips inject a larger total dislocation length.

Twinning was also found for the three indenters (Fig. 7). Our twinning findings for the spherical indenter are in agreement with previous reports on spherical indentation of  $\alpha$ -iron [30]. The substrate was found to have more atoms on twin boundaries for the case of the cube-corner tips, while the spherical indenter produced 30% less atoms in twin boundaries compared to SCC and RCC tips. In every case, the twin plane is a  $\langle 112 \rangle$  plane, as it is commonly found for bcc metals [59]. Due to the orientation of the pyramidal planes, twinning is largely localized in the region corresponding to the pyramidal plane whose normal vector is close to the  $[\bar{1}\bar{1}\bar{1}]$  direction.

## 4 Discussion

Unlike in large-scale nanoindentation behavior, nanocontact mechanics can be strongly influenced by adhesion between indenter and substrate, particularly with large surface area to volume ratio, clean surfaces, and ultra-high vacuum conditions. The seminal work by Landman et al. [37] showed the potential of molecular dynamics simulations to capture effects such as metallic bonding and substrate-to-tip atom transfer, also known as the tip-wetting or jump-to-contact phenomenon. The high surface energies associated with clean metal surfaces can lead to strong attractive forces between surfaces close to contact, particularly under conditions such as ultra-high vacuum, and if the attractive forces are strong enough, surface atoms jump from the surface to the tip. Although Fig. 3b clearly indicates an attractive interaction between the surface and the rounded tips prior to contact, no jump-to-contact was found. This is in agreement with a recent study of the influence of attractive forces in indentation simulation [60].

Although no significant differences were found between the pileups of the two cube-corner tips Fig. 4b and c, differences are noticeable below the surface. To begin with, the sharp indenter creates a considerable stress concentration at the tip that favors early dislocation generation by

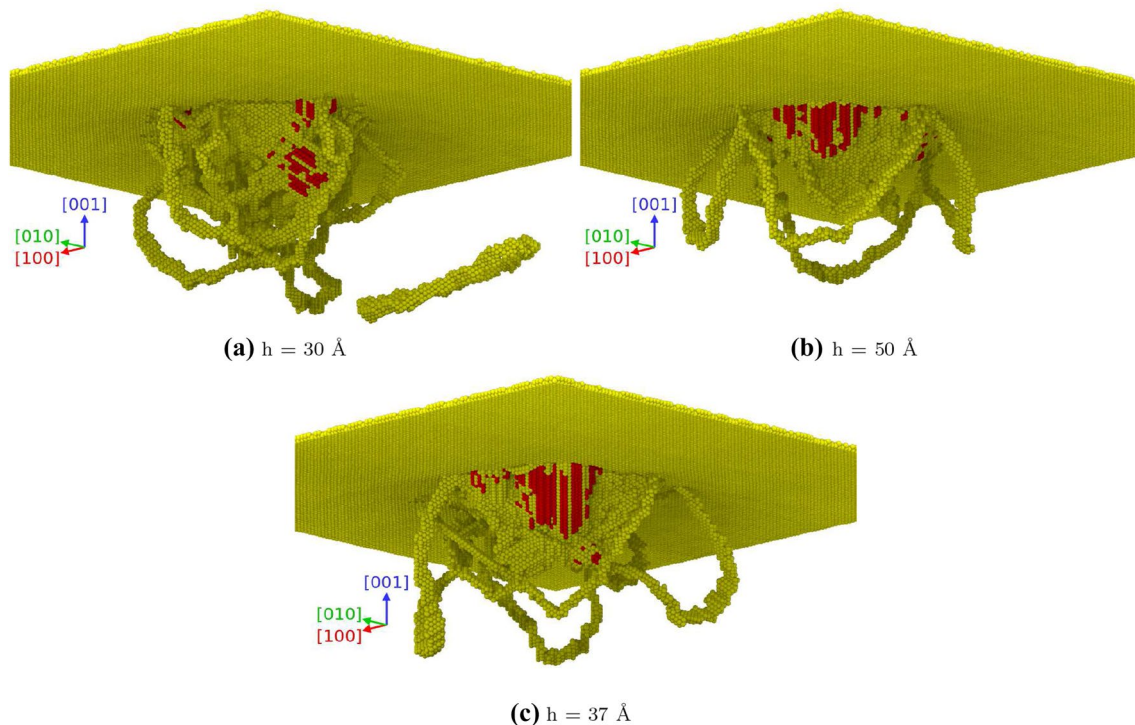


**Fig. 7** Example of twin boundaries (red) found in our simulations for a condition of equal displaced volume (different depth  $h$ ). **a** Spherical indenter (506 atoms). **b** Sharp cube-corner indenter (755 atoms). **c** Rounded cube-corner indenter (720 atoms)

heterogeneous nucleation at the surface, while the rounded cube-corner tip produces a stress distribution akin to that of the spherical indenter for a shallow penetration, generating dislocations by homogeneous nucleation. The qualitative analysis on Fig. 5b and c together with the quantitative analysis of Fig. 6 show that the sharp indenter caused less dislocations than the rounded indenters, endorsing the analysis of Gao et al. [61] and Zhu et al. [62]. Interestingly, though prismatic loop nucleation was found for our rounded cube-corner simulations, we verified that its formation gets delayed by the effect of the pyramid edges that tend to counterbalance cross-slip in the “lasso” mechanism [5], see supplementary movie S1. Ma et al [63] used a combination of experimental nanoindentation, AFM measurements, and FEM simulations to study the role of probe shape on the initiation of metal plasticity in nanoindentation, showing that changes in the shape of the indenter tips affect the dislocation nucleation stress; our results show that the influence can extend beyond the nucleation point.

Alhafez et al. [40] found that—in scratching—non-axisymmetric tips can be well approximated by cones if the cone opening angle is chosen as the equivalent opening angle of the non-axisymmetric tip, defined such that the ratio of indentation depth and cross-sectional area are identical. Following their treatment, we can compare the spherical and cube-corner indenters with a conical indenter with an *equivalent cone angle* [2]. It is defined by stipulating that the ratio of the normal contact area  $A_{\text{norm}}$  to the indentation depth  $h$  is identical to that of a cone. For a cone indented to depth  $h$ , it is

$$A_{\text{norm}} = \pi(h \tan \beta)^2. \quad (3)$$

Since for the cube-corner pyramid, it is

$$A_{\text{norm}} = \frac{3h^2}{(\tan \gamma \sin \gamma)}, \quad \text{with } \gamma = 90^\circ - 35.3^\circ, \quad (4)$$

the equivalent cone angle for the pyramid,  $\beta_{\text{scc}}$ , is given by

$$\tan \beta_{\text{scc}} = \sqrt{\frac{3}{\pi \tan \gamma \sin \gamma}} \quad (5)$$

and hence  $\beta_{\text{scc}} = 42.3^\circ$ . Since the pyramid is a self-similar geometry, the equivalent angle does not depend on the indentation depth  $h$ . Alhafez et al. [40] performed simulations with sharp cones of varying opening angle, and as  $\beta_{\text{scc}}$  is within those values, it is worth comparing with their results. The contact pressures reported in Fig. 3c are within the values reported in [40] for  $\beta = 45^\circ$ ; however, some differences arise when inspecting some characteristics of the deformation mechanisms. Not only pileup formation is different, due to the lack of axial symmetry in the cube-corner

tips, prismatic loops were found in our case, in agreement with [40] for  $\beta = 45^\circ$ .

It is important to highlight that the use of atomically rough indenters can produce results with significant deviations from predictions using continuum scale theories [38]. Similar conclusions apply for the use of smooth perfectly rigid indenters [36], and therefore, the choice of the indenter should be made after a thoughtful assessment of the implications of each election [64].

In Sect. 1, we proposed, as part of our objective, to question the typical hypothesis whether a sphere of similar radius to that of the experimental tip would provide a reasonable approximation to the real tip. The results presented here reveal that up to a penetration depth where the rounded cube-corner tip is identical to the sphere it provides a similar response for the elastic regime and also shows homogeneous nucleation of dislocations. However, for larger depths, where the planes of the cube-corner tips significantly interact with the substrate, important differences are found: the calculated hardness decreases and the formation of prismatic loops by the lasso mechanism gets delayed, that is, it occurs at a higher penetration. We attribute this delay to the effect of the edges of the pyramid; we observed that those dislocations that nucleate at, or get displaced to, the edges of the pyramid tend to be constrained by those edges to move along them, so while the screw components of the shear loops tend to attract each other by cross-slip, as explained by Remington and co-workers [5], the edges of the pyramid counterbalance that effect, and as the pyramid penetrates, it tends to separate the starting points of the shear loop from which the prismatic loop is trying to form. As the shear loops extend into the substrate, the effect of the edges is less prominent and cross-slip dominates, punching a prismatic loop, but at a higher penetration compared to the spherical case. Although the sharp cube-corner tip produces similar hardness and defective structures compared to its rounded counterpart, the loading curve is significantly different, where no clear signature of elastic regime can be found.

Our findings help to address, albeit in partial manner, some of the fundamental questions posed in the Introduction. Yet further efforts are needed to shed more light into nanocontact mechanics and plasticity at the nanoscale. Such efforts should include both experimental and simulation studies. In fact, Oliver et al. [65] are among those who had given the initial steps into that direction by performing one-to-one spatially matched experiment and atomistic simulations of nanometre-scale indentation; they reported that many features of the experiment were correctly reproduced by MD simulations. A more recent example can be found in the work by Vishnubhotla et al. [66].



## 5 Conclusions

Using classical molecular dynamics simulations, we study the influence of tip shapes on the nanoindentation response of a bcc single crystal. Three atomistically rough indenters were tested: a classical spherical tip, a sharp cube-corner tip, and a rounded cube-corner tip. Our main findings can be summarized as follows:

1. For shallow depths, the rounded pyramidal tip follows the elastic behavior of the spherical tip. However, as penetration goes beyond the radius, the slope of the loading curve for the rounded cube-corner tip is similar to that of the sharp tip, signaling the influence of the planes on the response.
2. The sharp tip favors heterogeneous nucleation of dislocations at the substrate surface, while the rounded tip favors homogeneous nucleation below the substrate surface.
3. For a given depth, sharp cube-corner tips produce a smaller total dislocation length and the radius of the plastic zone is significantly smaller for the sharp cube-corner tip.
4. For the same displaced volume, however, cube-corner tips produce a larger total dislocation length, in a slightly smaller plastic zone compared to the spherical tip.
5. For a penetration depth beyond the radius of the rounded cube-corner tip, atomic sharp pyramidal tips produce similar quantitative (hardness, dislocation density) and qualitative (pileup, dislocation arrangement) results compared to its rounded counterpart.
6. Tips with greater detail should be used in molecular dynamics studies in order to better capture various phenomena during the indentation process.

With the development of modern fabrication techniques (e.g., nanomachining with focused ion beam), great detail on the nanoindenter tip structure and shape can be achieved. Simulations like the ones presented here might aid in the design of tips and help in the characterization of the mechanics of nanocontact for such new geometries.

**Acknowledgements** HMU acknowledges support by the Deutsche Forschungsgemeinschaft (DFG, German Research Foundation)—Project Number 172116086—SFB 926. CJR and MCZ acknowledge support by ANPCyT PICT-2015-0342, SiiP-UNCuyo-2019-M088, a donation by the Nvidia Corporation, and computational resources at TOKO-FCEN-UNCuyo cluster. EMB thanks funding from SiiP-UNCuyo-2019-2021 grant. The work by MCZ was supported by an EVC scholarship from Consejo Interuniversitario Nacional - Argentina.

## References

1. Johnson, K.L.: Contact Mechanics. Cambridge University Press, Cambridge (1985)
2. Fischer-Cripps, A.C.: Nanoindentation, 2nd edn. Springer, New York (2004)
3. Armstrong, R.W., Elban, W.L., Walley, S.M.: Elastic, plastic, cracking aspects of the hardness of materials. *Int. J. Mod. Phys. B* **27**, 1330004 (2013)
4. Armstrong, R.W., Walley, S.M., Elban, W.L.: Crystal indentation hardness. *Crystals* **7**, 21 (2017)
5. Remington, T.P., Ruestes, C.J., Bringa, E.M., Remington, B.A., Lu, C.H., Kad, B., Meyers, M.A.: Plastic deformation in nanoindentation of tantalum: a new mechanism for prismatic loop formation. *Acta Mater.* **78**, 378–393 (2014)
6. Ruestes, C.J., Stukowski, A., Tang, Y., Tramontina, D.R., Erhart, P., Remington, B.A., Urbassek, H.M., Meyers, M.A., Bringa, E.M.: Atomistic simulation of tantalum nanoindentation: effects of indenter diameter, penetration velocity, and interatomic potentials on defect mechanisms and evolution. *Mater. Sci. Eng. A* **613**, 390–403 (2014)
7. Ruestes, C.J., Bringa, E.M., Gao, Y., Urbassek, H.M.: Molecular dynamics modeling of nanoindentation. In: Tiwari, A., Nataraajan, S. (eds.) *Applied Nanoindentation in Advanced Materials*, Chapter 14, pp. 313–345. Wiley, Chichester (2017)
8. Ruestes, C.J., Alabd Alhafez, I., Urbassek, H.M.: Atomistic studies of nanoindentation—A review of recent advances. *Crystals* **7**, 293 (2017b)
9. Van Vliet, K.J., Li, J., Zhu, T., Yip, S., Suresh, S.: Quantifying the early stages of plasticity through nanoscale experiments and simulations. *Phys. Rev. B* **67**, 104105 (2003)
10. Ma, X.-L., Yang, W.: Molecular dynamics simulation on burst and arrest of stacking faults in nanocrystalline Cu under nanoindentation. *Nanotechnology* **14**, 1208 (2003)
11. Zhu, T., Li, J., Van Vliet, K.J., Ogata, S., Yip, S., Suresh, S.: Predictive modeling of nanoindentation-induced homogeneous dislocation nucleation in copper. *J. Mech. Phys. Sol.* **52**, 691 (2004)
12. Liang, H., Woo, C.H., Huang, H., Ngan, A.H.W., Yu, T.X.: Crystalline plasticity on copper (001), (110), and (111) surfaces during nanoindentation. *Comput. Model. Eng. Sci.* **6**, 105 (2004)
13. Asenjo, A., Jaafar, M., Carrasco, E., Rojo, J.M.: Dislocation mechanisms in the first stage of plasticity of nanoindented Au (111) surfaces. *Phys. Rev. B* **73**, 075431 (2006)
14. Tsuru, T., Shibutani, Y.: Anisotropic effects in elastic and incipient plastic deformation under (001), (110), and (111) nanoindentation of Al and Cu. *Phys. Rev. B* **75**, 035415 (2007)
15. Ju, S.-P., Wang, C.-T., Chien, C.-H., Huang, J.C., Jian, S.-R.: The nanoindentation responses of nickel surfaces with different crystal orientations. *Mol. Simul.* **33**, 905 (2007)
16. Carrasco, E., Rodríguez de la Fuente, O., Rojo, J.M.: Dislocation emission at the onset of plasticity during nanoindentation in gold. *Philos. Mag.* **88**, 281 (2008)
17. Ziegenhain, G., Urbassek, H.M.: Effect of material stiffness on hardness: a computational study based on model potentials. *Philos. Mag.* **89**, 2225–2238 (2009)
18. Ziegenhain, G., Hartmaier, A., Urbassek, H.M.: Pair vs many-body potentials: influence on elastic and plastic behavior in nanoindentation of fcc metals. *J. Mech. Phys. Sol.* **57**, 1514–1526 (2009)
19. Ziegenhain, G., Urbassek, H.M., Hartmaier, A.: Influence of crystal anisotropy on elastic deformation and onset of plasticity in nanoindentation: a simulational study. *J. Appl. Phys.* **107**, 061807 (2010)

20. Paul, W., Oliver, D., Miyahara, Y., Grütter, P.H.: Minimum threshold for incipient plasticity in the atomic-scale nanoindentation of Au(111). *Phys. Rev. Lett.* **110**, 135506 (2013)
21. Gao, Y., Ruestes, C.J., Tramontina, D.R., Urbassek, H.M.: Comparative simulation study of the structure of the plastic zone produced by nanoindentation. *J. Mech. Phys. Sol.* **75**, 58–75 (2015)
22. Hagelaar, J.H.A., Bitzek, E., Flipse, C.F.J., Gumbsch, P.: Atomistic simulations of the formation and destruction of nanoindentation contacts in tungsten. *Phys. Rev. B* **73**, 045425 (2006)
23. Biener, M.M., Biener, J., Hodge, A.M., Hamza, A.V.: Dislocation nucleation in bcc Ta single crystals studied by nanoindentation. *Phys. Rev. B* **76**, 165422 (2007)
24. Alcalá, J., Dalmau, R., Franke, O., Biener, M., Biener, J., Hodge, A.: Planar defect nucleation and annihilation mechanisms in nanocontact plasticity of metal surfaces. *Phys. Rev. Lett.* **109**, 075502 (2012)
25. Christopher, D., Smith, R., Richter, A.: Atomistic modelling of nanoindentation in Fe and Ag. *Nanotechnology* **12**, 372 (2001)
26. Smith, R., Christopher, D., Kenny, S.D., Richter, A., Wolf, B.: Defect generation and pileup of atoms during nanoindentation of Fe single crystals. *Phys. Rev. B* **67**, 245405 (2003)
27. Lu, C., Gao, Y., Michal, G., Deng, G., Huynh, N.N., Zhu, H., Liu, X., Tieu, A.K.: Experiment and molecular dynamics simulation of nanoindentation of body centered cubic iron. *J. Nanosci. Nanotechnol.* **9**, 7307 (2009a)
28. Lu, C., Gao, Y., Michal, G., Huynh, N.N., Zhu, H.T., Tieu, A.K.: Atomistic simulation of nanoindentation of iron with different indenter shapes. *Proc. IME J.* **223**, 977 (2009b)
29. Kumar, N.N., Tewari, R., Durgaprasad, P.V., Dutta, B.K., Dey, G.K.: Active slip systems in bcc iron during nanoindentation: a molecular dynamics study. *Comput. Mater. Sci.* **77**, 260 (2013)
30. Gao, Y., Ruestes, C.J., Urbassek, H.M.: Nanoindentation and nanoscratching of iron: atomistic simulation of dislocation generation and reactions. *Comput. Mater. Sci.* **90**, 232–240 (2014)
31. Alabd Alhafez, I., Ruestes, C.J., Bringa, E.M., Urbassek, H.M.: Influence of pre-existing plasticity on nanoindentation—An atomistic analysis of the dislocation fields produced. *J. Mech. Phys. Solids* **132**, 103674 (2019a)
32. Verkhovtsev, A.V., Yakubovich, A.V., Sushko, G.B., Hanauske, M., Solov'yov, A.V.: Molecular dynamics simulations of the nanoindentation process of titanium crystal. *Comput. Mater. Sci.* **76**, 20–26 (2013)
33. Alabd Alhafez, I., Ruestes, C.J., Gao, Y., Urbassek, H.M.: Nanoindentation of hcp metals: a comparative simulation study of the evolution of dislocation networks. *Nanotechnology* **27**, 045706 (2016)
34. Avila, K.E., Küchemann, S., Alabd Alhafez, I., Urbassek, H.M.: Shear-transformation-zone activation during loading and unloading in nanoindentation of metallic glasses. *Materials* **12**, 1477 (2019)
35. Alabd Alhafez, I., Ruestes, C.J., Bringa, E.M., Urbassek, H.M.: Nanoindentation into a high-entropy alloy—An atomistic study. *J. Alloys Compd.* **803**, 618–624 (2019b)
36. Kelchner, C.L., Plimpton, S.J., Hamilton, J.C.: Dislocation nucleation and defect structure during surface indentation. *Phys. Rev. B* **58**, 11085–11088 (1998)
37. Landman, U., Luedtke, W.D., Burnham, N.A., Colton, R.J.: Atomistic mechanisms and dynamics of adhesion, nanoindentation, and fracture. *Science* **248**, 454 (1990)
38. Luan, B., Robbins, M.O.: The breakdown of continuum models for mechanical contacts. *Nature* **435**, 929 (2005)
39. Wagner, R.J., Ma, L., Tavazza, F., Levine, L.E.: Dislocation nucleation during nanoindentation of aluminum. *J. Appl. Phys.* **104**, 114311 (2008). <https://doi.org/10.1063/1.3021305>
40. Alabd Alhafez, I., Brodyanski, A., Kopnarski, M., Urbassek, H.M.: Influence of tip geometry on nanoscratching. *Tribol. Lett.* **65**, 26 (2017)
41. Komanduri, R., Chandrasekaran, N., Raff, L.M.: Md simulation of atomic-scale friction. *Phys. Rev. B* **61**, 14007 (2000)
42. Kenny, S.D., Mulliah, D., Sanz-Navarro, C.F., Smith, R.: Molecular dynamics simulations of nanoindentation and nanotribology. *Philos. Trans. R. Soc. A* **363**, 1949–1959 (2005)
43. Jun, S., Lee, Y., Kim, S.Y., Im, S.: Large-scale molecular dynamics simulations of Al(111) nanoscratching. *Nanotechnology* **15**, 1169–1174 (2004)
44. Yaghoobi, M., Voyiadjis, G.Z.: Effect of boundary conditions on the MD simulation of nanoindentation. *Comput. Mater. Sci.* **95**, 626–636 (2014)
45. Mendeleev, M.I., Han, S., Srolovitz, D.J., Ackland, G.J., Sun, D.Y., Asta, M.: Development of new interatomic potentials appropriate for crystalline and liquid iron. *Philos. Mag.* **83**, 3977–3994 (2003)
46. Banerjee, S., Naha, S., Puri, I.K.: Molecular simulation of the carbon nanotube growth mode during catalytic synthesis. *Appl. Phys. Lett.* **92**, 233121 (2008)
47. Allen, M.P., Tildesley, D.J. (eds.): *Computer Simulation of Liquids* (Clarendon, Oxford, 1987)
48. Plimpton, S.: Fast parallel algorithms for short-range molecular dynamics. *J. Comput. Phys.* **117**, 1–19 (1995)
49. Stukowski, A.: Visualization and analysis of atomistic simulation data with OVITO—The Open Visualization Tool. *Model. Simul. Mater. Sci. Eng.* **18**, 015012 (2010)
50. Stukowski, A., Albe, K.: Extracting dislocations and non-dislocation crystal defects from atomistic simulation data. *Model. Simul. Mater. Sci. Eng.* **18**, 085001 (2010)
51. Stukowski, A., Bulatov, V.V., Arsenlis, A.: Automated identification and indexing of dislocations in crystal interfaces. *Model. Simul. Mater. Sci. Eng.* **20**, 085007 (2012)
52. Stukowski, A.: Structure identification methods for atomistic simulations of crystalline materials. *Model. Simul. Mater. Sci. Eng.* **20**, 045021 (2012)
53. Stukowski, A., Arsenlis, A.: On the elastic-plastic decomposition of crystal deformation at the atomic scale. *Model. Simul. Mater. Sci. Eng.* **20**, 035012 (2012)
54. Gerberich, W.W., Nelson, J., Lilleodden, E., Anderson, P., Wyrobek, J.: Indentation induced dislocation nucleation: the initial yield point. *Acta Mater.* **44**, 3585–3598 (1996)
55. Li, J., Van Vliet, K.J., Zhu, T., Yip, S., Suresh, S.: Atomistic mechanisms governing elastic limit and incipient plasticity in crystals. *Nature* **418**, 307–310 (2002)
56. Gunkelmann, N., Bringa, E.M., Kang, K., Ackland, G.J., Ruestes, C.J., Urbassek, H.M.: Polycrystalline iron under compression: plasticity and phase transitions. *Phys. Rev. B* **86**, 144111 (2012)
57. Yao, W.Z., Krill III, C.E., Albinski, B., Schneider, H.-C., You, J.H.: Plastic material parameters and plastic anisotropy of tungsten single crystal: a spherical micro-indentation study. *J. Mater. Sci.* **49**, 3705 (2014)
58. Terentyev, D.A., Osetsky, Y.N., Bacon, D.J.: Effects of temperature on structure and mobility of the <1 0 0> edge dislocation in body-centred cubic iron. *Acta Mater.* **58**, 2477 (2010)
59. Kelly, A., Knowles, K.M.: *Crystallography and Crystal Defects*, 2nd edn. Wiley, Chichester (2012)
60. Alabd Alhafez, I., Urbassek, H.M.: Influence of tip adhesion on nanoindentation and scratching. *Model. Simul. Mater. Sci. Eng.* **27**, 065014 (2019)
61. Gao, Y., Lu, C., Huynh, N.N., Michal, G., Zhu, H.T., Tieu, A.K.: Molecular dynamics simulation of effect of indenter shape on nanoscratch of Ni. *Wear* **267**, 1998 (2009)
62. Zhu, P.-Z., Hu, Y.-Z., Wang, H., Ma, T.-B.: Study of effect of indenter shape in nanometric scratching process using molecular dynamics. *Mater. Sci. Eng. A* **528**, 4522 (2011)

63. Ma, L., Morris, D.J., Jennerjohn, S.L., Bahr, D.F., Levine, L.E.: The role of probe shape on the initiation of metal plasticity in nanoindentation. *Acta Mater.* **60**, 4729–4739 (2012)
64. Goel, S., Cross, G., Stukowski, A., Gamsjäger, E., Beake, B., Agrawal, A.: Designing nanoindentation simulation studies by appropriate indenter choices: case study on single crystal tungsten. *Comput. Mater. Sci.* **152**, 196–210 (2018)
65. Oliver, D., Paul, W., El Ouali, M., Hagedorn, T., Miyahara, Y., Qi, Y., Grütter, P.: One-to-one spatially matched experiment and atomistic simulations of nanometre-scale indentation. *Nanotechnology* **25**, 025701 (2013)
66. Vishnubhotla, S.B., Chen, R., Khanal, S.R., Hu, X., Martini, A., Jacobs, T.D.B.: Matching atomistic simulations and in situ experiments to investigate the mechanics of nanoscale contact. *Tribol. Lett.* **67**, 97 (2019)

**Publisher's Note** Springer Nature remains neutral with regard to jurisdictional claims in published maps and institutional affiliations.